Chemical Engineering Journal 388 (2020) 124134

Contents lists available at ScienceDirect

Chemical Engineering Journal

journal homepage: www.elsevier.com/locate/cej

Short communication

Revelation of ferrate(VI) unimolecular decay under alkaline conditions: Investigation of involvement of Fe(IV) and Fe(V) species

Cong Luo[a], Mingbao Feng[b], Virender K. Sharma[b,*], Ching-Hua Huang[a,*]

[a] School of Civil and Environmental Engineering, Georgia Institute of Technology, Atlanta, GA 30332, USA
[b] Department of Environment and Occupational Health, School of Public Health, Texas A&M University, College Station, TX 77843, USA

HIGHLIGHTS

- Fe(VI) decays by unimolecular mechanism under alkaline condition (pH 9.0–10.0).
- Unimolecular decay occurs via water attack (WA) mechanism based on DFT calculation.
- Kinetic modeling and DFT suggest involvement of Fe(V) and Fe(IV) intermediate species.
- Fe(VI) self-decay generates H_2O_2, which was quantified experimentally.
- Successful kinetic modeling of H_2O_2 formation and Fe(VI) disappearance in Fe(VI) decay.

GRAPHICAL ABSTRACT

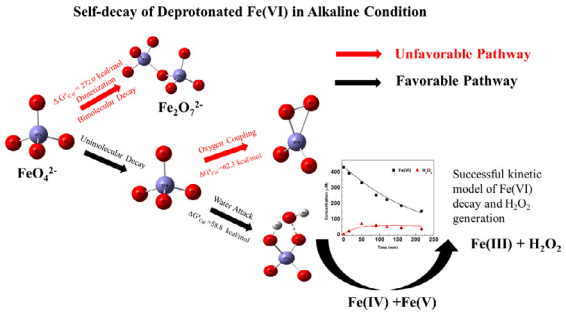

ARTICLE INFO

Keywords:
Ferrates
Self-decay
Water attack
Kinetic simulation
DFT calculation

ABSTRACT

The kinetics and mechanisms of self-decay of ferrate(VI) ($Fe^{VI}O_4^{2-}$, Fe(VI)) over the entire pH range from acidic to basic pH range need to be understood to assess the ability of Fe(VI) to oxidize pollutants at different pHs. Mechanism of self-decay of Fe(VI) has been extensively examined under acidic to neutral pH conditions. However, Fe(VI) self-decay at alkaline pH (e.g., pH 9.0 or higher) is poorly understood. This study performed kinetic and modeling studies of the Fe(VI) decay at pH 9.0 and 10.0. Our research reveals that the decay of Fe (VI) follows first-order kinetics (i.e., unimolecular decay) at pH 9.0 and 10.0 and the order changes to 3/2-order at pH 7.0 due to the different species of Fe(VI) (FeO_4^{2-} versus $HFeO_4^-$). Results of unimolecular decay mechanism through water attack (WA) are supported by density functional theory (DFT) calculations, which indicate unfavorable dimerization of FeO_4^{2-} through oxo-coupling (OC) under alkaline conditions. The WA on the monomeric FeO_4^{2-} is proposed due to its lower activation barrier compared to OC. Kinetic simulation of Fe(VI) decay involving Fe(V) and Fe(IV) successfully predicts Fe(VI) disappearance and H_2O_2 generation (a product) under varied conditions. The decay of FeO_4^{2-} is different from the second-order kinetics of protonated Fe(VI) species (H_2FeO_4 and $HFeO_4^-$). Our results will aid in comprehending oxidation power of Fe(VI) in degrading pollutants under alkaline conditions.

1. Introduction

Over the past decade, ferrate(VI) ($Fe^{VI}O_4^{2-}$, Fe(VI)), a powerful oxidizing agent with a standard potential of 2.2 V in acid solution and 0.7 V at alkaline condition [1], has emerged as a novel oxidant to remove contaminants from water [2–5]. The oxidation ability to remove

* Corresponding authors.
E-mail addresses: vsharma@tamu.edu (V.K. Sharma), ching-hua.huang@ce.gatech.edu (C.-H. Huang).

https://doi.org/10.1016/j.cej.2020.124134
Received 4 October 2019; Received in revised form 6 January 2020; Accepted 13 January 2020
Available online 28 January 2020
1385-8947/

pollutants is generally determined by the competing rate constants of the reaction between Fe(VI) with pollutants (X) (Reaction R(1)) and simultaneous self-decay of Fe(VI) (Reaction R(2) or Reaction R(3)):

$$Fe(VI) + X \rightarrow Products \quad (R1)$$

$$Fe(VI) + H_2O \rightarrow Products \quad (R2)$$

$$Fe(VI) + Fe(VI) \rightarrow Products \quad (R3)$$

It is imperative to know whether the self-decay is first-order (Reaction R(2)), second-order (Reaction R(3)), or both to assess the ability of Fe(VI) to oxidize pollutants [6]. For example, if Fe(VI) self-decay is first-order, the half-life of Reaction R(2) would be independent of Fe(VI) concentration. Comparatively, the half-life of Reaction R(3) would be inversely related to Fe(VI) concentration. The rates of the reactions of Fe(VI) with pollutants (i.e., Reaction R(1)) are highly pH-dependent in the acidic to basic pH range. The oxidative removal of pollutants by Fe(VI) over the entire pH range may be understood by knowing the pH dependence of the self-decay of Fe(VI). Many studies have been conducted in acidic to neutral pH on the decay of Fe(VI) in water, but similar information in basic medium is scarce. Information on the self-decay of Fe(VI) under basic pH has become important in our research, in which we have sought to remove pharmaceuticals from the alkaline systems (e.g., hydrolyzed human urine samples [7]).

Fe(VI) is unstable in aqueous solution under acidic conditions [8,9] and could react with H_2O to produce Fe(III), O_2 [10] and H_2O_2 [11] as the final products. The mechanism for Fe(VI) self-decomposition at very acidic condition (e.g., pH 1.0–3.0) has been proposed recently [12]. It includes the formation of a diferrate(VI) and subsequent intramolecular oxo-coupling, which results in the production of O_2 and diferryl(IV) species, on the basis of the study of ^{18}O isotope effects on kinetics and computational method based on the density functional theory (DFT). This mechanism has been extended to near-neutral pH (pH 1.0–8.3) with a minor modification that was changed from direct O_2 formation to H_2O_2 stripping as the intermediate step to form diferryl(VI), according to the experimental evidence of H_2O_2 generation [11]. Recently, Chen and co-workers [13] also confirmed the second-order reaction of Fe(VI) decay at pH 8.0, based on the linear relationship between the initial Fe(VI) decay rate and $[Fe(VI)]^2$. However, the mechanism of Fe(VI) self-decay at alkaline conditions (e.g., pH 9.0 or 10.0) has been poorly understood even though the optimal working pH for Fe(VI) may be at 9.0 after compromising between the Fe(VI)'s self-decay rate and oxidizing capability [14,15].

Herein, the reaction kinetics of Fe(VI) self-decay at alkaline conditions (particularly pH 9.0) were carefully examined experimetnally, and the mechanism was proposed and validated by DFT calculations. A kinetic model including Fe(VI) and intermediate iron species (i.e., Fe(V) and Fe(IV)) was developed to predict Fe(VI) decay and H_2O_2 generation at pH 9.0 to quantitatively assess the involvement of the intermediate iron species.

2. Materials and methods

The self-decay of Fe(VI) (initial concentration was 107.0–695.0 μM for long duration experiments and 101.0–1220.0 μM for initial rate method) at pH 9.0 or 10.0 (in 10.0 mM phosphate buffer) was studied in constantly stirred batch reactors at 25 °C and monitored by UV–vis spectrophotometry. The kinetic model simulations were conducted using Simbiology Version 5.7 in MATLAB 2018 (The Math Works, Inc.). Details of experimental and computational methods are provided in the Supporting Information (SI) Text S1.

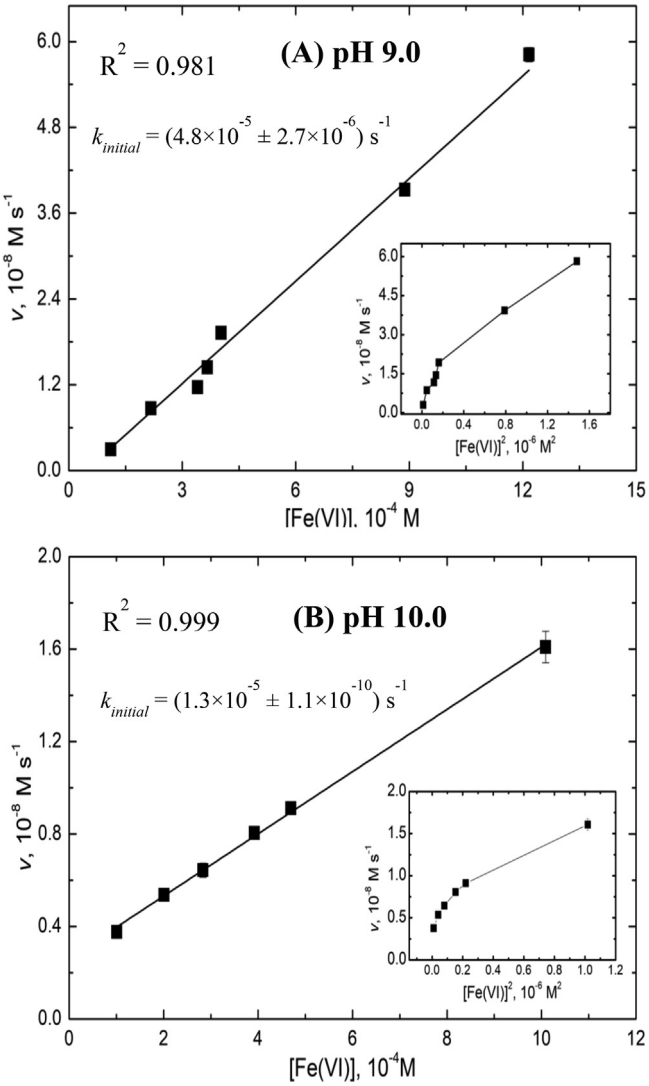

Fig. 1. Relationship between the initial Fe(VI) decay rate and initial [Fe(VI)] at pH 9.0 (A) and 10.0 (B) in 10.0 mM phosphate buffer. $[Fe(VI)]_0$ = 101.0–1220.0 μM; n = 2; Insets show the corresponding plot of initial rate *vs.* $[Fe(VI)]^2$.

3. Results and discussion

3.1. Self-decay kinetics of Fe(VI) under alkaline conditions

According to the speciation of Fe(VI) [16], deprotonated Fe(VI) (FeO_4^{2-}) is the major species (98%) at pH 9.0 ($HFeO_4^- \rightleftharpoons H^+ + FeO_4^{2-}$, pK_{a3} = 7.23 [17]). The self-decay of Fe(VI) was studied at pH 9.0 with the initial concentrations (i.e., $[Fe(VI)]_0$) ranging from 107 to 434 μM (Fig. S1). Most previous research proposed a 2nd-order reaction with respect to Fe(VI) for its decay [11,12,18]. However, the Fe(VI) decay data fitted better with the 1st-order kinetics with more consistent rate constants and higher R^2 values compared to the 2nd-order kinetics (See Table S1). The mixed 1st- and 2nd-order kinetics were also utilized to simulate the Fe(VI) decay data but could not obtain meaningful rate constants (see Text S1.2 and Table S2), indicating that the assumption (i.e., FeO_4^{2-} can initiate 1st- and 2nd-order decays in parallel) could not be applied in this case.

Next, the method of initial rate was used to determine the order (n) of the self-decay of Fe(VI) (Text S1.3). In Fig. 1A, the linear relationship was observed only between the initial rate and [Fe(VI)] at pH 9.0, which was consistent with the rate law $v = k_{initial}[FeO_4^{2-}]$ ($k_{initial}$ =

$4.8 \times 10^{-5}\ s^{-1}$ at pH 9.0). As Fig. 1A inset shows, no linearity was seen between the initial rate and $[Fe(VI)]^2$, further suggesting that the rate was first-order with respect to [Fe(VI)]. The same phenomenon was also observed at pH 10.0 (Fig. 1B). The above evidence strongly suggested that Fe(VI) decomposition under alkaline conditions (pH 9.0 and 10.0), where FeO_4^{2-} dominates, followed the 1st-order kinetics rather than the 2nd-order decay kinetics proposed in other previous studies [11,18]. Therefore, it is plausible that the protonation of Fe(VI) could alter the decay reaction order, i.e., the deprotonated form follows 1st-order reaction (unimolecular decay) and the protonated form follows 2nd-order reaction (bimolecular decay).

To test the above hypothesis, Fe(VI) decay at pH 7.5 was investigated at varied initial concentrations of Fe(VI) because deprotonated and mono-protonated Fe(VI) (53% FeO_4^{2-} and 47% $HFeO_4^-$) coexisted under such condition. When attempting to fit the data with 1st- or 2nd-order kinetics, neither could fully depict satisfactorily the Fe (VI) self-decay (Fig. S2 and Table S1). For 1st-order reaction, the rate constant was not significantly affected by the initial Fe(VI) concentrations but R^2 deteriorated to 0.91 when $[Fe(VI)]_0$ was increased to 695 μM. For 2nd-order reaction, the better R^2 values were observed but the rate constants were changed from 1.10 to 5.51 $M^{-1}\cdot s^{-1}$ at different levels of $[Fe(VI)]_0$. Thus, both kinetic models failed to describe Fe(VI) decay at pH 7.5.

The order of this reaction was then determined by the method described in Text S1.2 and was found to be ~3/2 (shown by the regression slope in Fig. S3A). After fitting the data into the 3/2-order kinetics, the better values of R^2 were obtained (i.e., 0.94–0.99) and the more consistent rate constants (an average value of $6.23 \times 10^{-2}\ s^{-1}$ with 28.8% deviation) were observed (Table S1). This phenomenon can be explained by the coexistence of similar concentrations of deprotonated and mono-protonated Fe(VI) species. Similarly, previous studies have attempted to use the mixed 1st- and 2nd-order kinetics to describe Fe(VI) self-decay under acidic-to-neutral conditions and found that the 2nd-order kinetics began to dominate the decay pathway as pH was decreased [10,19].

3.2. Mechanistic investigation based on the DFT calculations

Since dimerization of two Fe(VI) to form diferrate(VI) has been proposed as the major step to initiate the bimolecular decay under acidic-to-neutral conditions [11,12,20], unimolecular decay of Fe(VI) under alkaline condition is expected to follow a different decay pathway. The DFT calculations were employed to elucidate the Fe(VI) decay mechanism under this condition.

Table 1 shows the optimized geometries of different Fe(VI) species in aqueous solution. The calculated Fe-O distance (1.65 Å) and Fe-O-Fe angle (109.5°) for FeO_4^{2-} in water were in good agreement with the X-ray structure of K_2FeO_4 [21]. By comparing the LUMO energy levels based on the B3LYP method, it was evident that the oxidizing ability of Fe(VI) species became stronger upon protonation because of the increased electron accepting ability of H_2FeO_4 and $HFeO_4^-$, which agrees well with the pH dependence of Fe(VI) reactivity derived from experiments [22]. These results validated the use of DFT/B3LYP method combined with mixed basis sets. Furthermore, protonation influenced the bond length between Fe and O. Compared to the 1Fe-2O distance of 1.65 Å in FeO_4^{2-}, the corresponding 1Fe-2O(H) increased to 1.742 Å and 1.801 Å in H_2FeO_4 and $HFeO_4^-$ after protonation. Such increase in 1Fe-2O(H) distance resulted in much easier bond-breaking reactions in aqueous phase. The calculated 1Fe-2O(H) dissociation energy also increased with deprotonation, which indicated that 1Fe-2O(H) bond became more difficult to break at higher pH.

The calculated free energy barriers (Scheme S1) suggested that the thermodynamics of condensation and dimerization changed from favorable (-1.0 kcal/mol, compared to −1.3 kcal/mol calculated by Sarma et al. [12]) to unfavorable (272.1 kcal/mol) along the deprotonation. This is due to FeO_4^{2-} species having (i) a shorter Fe-O(H) distance and a higher bond dissociation energy, and (ii) a stronger intermolecular electrostatic repulsion. Ma and coworkers [23] reported an accelerating effect of Ca^{2+} on Fe(VI) decay at pH 9–10, and demonstrated unfavorable dimerization of FeO_4^{2-} species unless in the help of metal cations such as Ca^{2+} to bridge two FeO_4^{2-} ions. Note that Sarma et al. [12] also found that, at very low pH (~1), Fe(VI) decay was ruled by 1st-order kinetics and the calculated free energy for the formation of diferrate(VI) became positive (9.27 kcal/mol), indicating unfavorable situation to initiate dimerization for tri-protonated Fe(VI) ($H_3FeO_4^+$).

Fe(VI) self-decay process in aqueous phase can also be regarded as water oxidation, where the rate-limiting O-O bond formation is critical to elucidate the reaction pathway. Formation of O-O bond in Fe(VI) can be achieved either through oxo-coupling (OC) in Fe(VI)'s oxo ligands or water attack (WA) reaction that may involve high-energy electrophilic intermediates [24–28]. Both possible mechanisms were examined by locating their corresponding transition states (TS) and perform intrinsic reaction coordinate (IRC) analysis using the DFT method. In Table 2, monomeric Fe(VI) reaction pathways were designated according to spin state, protonation level and mechanisms of O-O bond formation. For example, the TS for OC with the monoprotonated $HFeO_4^-$ via the unrestricted triplet is designated as ^{3}1OC. The activation barriers noted as $\Delta G^{\ddagger}_{Cal}$ are also shown in Table 2. The results showed that O-O bond formation was more favorable for $HFeO_4^-$ with the lower $\Delta G^{\ddagger}_{Cal}$ values observed in ^{3}1OC (42.5 kcal/mol) and ^{3}1WA (25.1 kcal/mol) in comparison to the deprotonated FeO_4^{2-} (62.3 kcal/mol in ^{3}0OC or and

Table 1
Optimized geometries of Fe(VI) species based on DFT calculations (bond length in Å).

Ferrate	H_2FeO_4	$HFeO_4^{-1}$	FeO_4^{-2}
Optimized Geometry	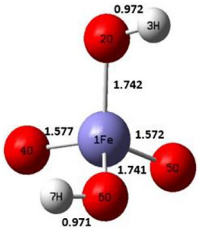	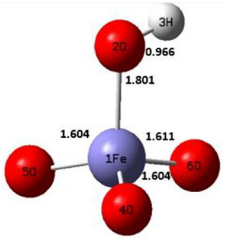	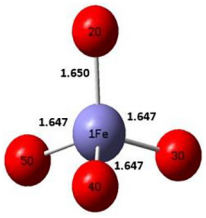
Charge	0	−1	−2
Spin State	Triplet	Triplet	Triplet
Relative Gibbs Free Energy (Kcal/mol)	0	261.7	555.0
1Fe-2O(H) Bond Dissociation Energy (Kcal/mol)	36.3	45.8	53.2
LUMO (eV)	−5.15	−3.44	−1.95
HOMO (eV)	−8.99	−7.32	−7.09

Table 2
Free energy barriers to oxo-coupling (OC) and water attack (WA) calculated for monoprotonated Fe(VI) ($HFeO_4^-$) and deprotonated Fe(VI) (FeO_4^{2-}).

Ferrate	^{3}1WA	^{3}1OC	^{3}0WA	^{3}0OC
Transition State	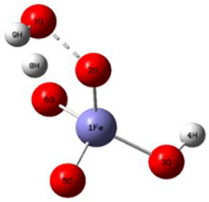	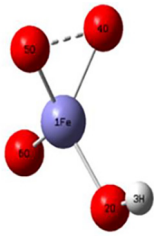	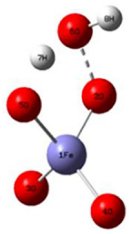	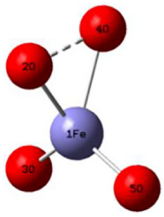
$\Delta G^{\ddagger}_{Cal}$ (Kcal/mol)	25.1	42.5	58.8	62.3

58.8 kcal/mol in ^{3}0WA). A similar result was also observed when comparing the O-O bond formation for $H_3FeO_4^+$ and H_2FeO_4, where $\Delta G^{\ddagger}_{Cal}$ value increased with the decreasing protonation levels [12]. On the other hand, it is notable that WA for FeO_4^{2-} had relatively lower activation barrier in TS compared to OC (58.8 *vs.* 62.3 kcal/mol). A similar trend was also reported previously for $HFeO_4^-$ (27.8 kcal/mol (WA) *vs.* 37.4 kcal/mol (OC) [13]), H_2FeO_4 (30.2 kcal/mol (WA) *vs.* 41.0 kcal/mol (OC) [12]) and $H_3FeO_4^+$ (20.8 kcal/mol (WA) *vs.* 24.5 kcal/mol (OC) [12]). These findings confirmed that, unlike OC, which occurred in diferrate molecules at lower pH, monomeric deprotonated ferrate (FeO_4^{2-}) in alkaline solution was more likely to initiate WA to complete the O-O bond formation. The products generated from WA were also analyzed in Text S2.

3.3. Kinetic model of Fe(VI) self-decay: Involvement of Fe(IV) and Fe(V)

A kinetic model including Equations 1–10 in Scheme 1 and Table 3 was used to simulate the Fe(VI) decay behavior at pH 9.0 under various experimental conditions. Fe(VI), as well as H_2O_2 (one of the major end products of Fe(VI) decay), were experimentally measured and the results were used to validate the kinetic model. Even though FeO_4^{2-} is the dominant species at pH 9.0 (98% FeO_4^{2-} *vs.* 2% $HFeO_4^-$), the contribution of $HFeO_4^-$ may not be negligible if it has relatively high reaction rates with substrates. Therefore, $HFeO_4^-$ was included in Equations 1b, 2b, and 7b to fully delineate the species-specific kinetic behaviors of ferrates in the oxidation system.

Equation 1a represents the initiation of FeO_4^{2-} self-decomposition from WA, generating one Fe(IV) species and one H_2O_2. This reaction was identified in our study and occurred via 1st-order kinetics with its $k_{initial}$ to be 4.8 × 10^{-5} s^{-1} (in Fig. 1). According to the proposed reaction pathway in Scheme S2, WA can be deemed as the addition of one ·OH and one proton to two separate oxygen ligands in Fe(VI) to form a hydrolyzed Fe(V) intermediate species. After stripping one H_2O_2 via

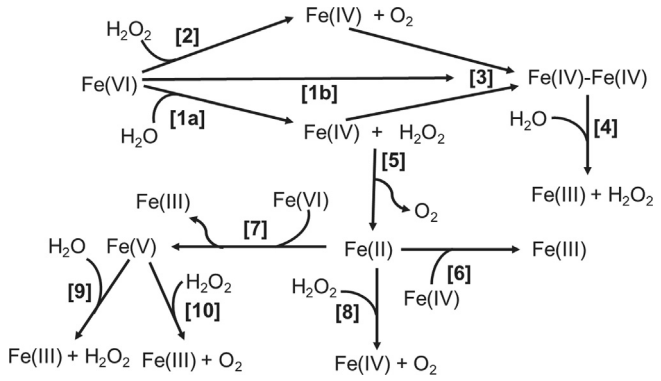

Scheme 1. Reaction scheme of self-decay of Fe(VI) at pH 9.0. (Note: The numbers in the brackets correspond to the reactions shown in Table 3).

one electron transfer from the central iron atom, one deprotonated Fe (IV) species is formed. Equation 1b, on the other hand, shows the bimolecular decay of $HFeO_4^-$ via OC, which has been carefully examined previously [11]. It's possible that Fe(VI) may react with H_2O_2 (Eqs. 2a and b) and their species-specific rate constants were evaluated and modeled by Rush et al. [20] according to experimentally measured pH-dependent apparent rate constants. The reaction rate constant between $HFeO_4^-$ and H_2O_2 was determined to be 1.7 × 10^2 $M^{-1}{\cdot}s^{-1}$ (Eq. 2b). However, negligible reaction between FeO_4^{2-} and H_2O_2 was found in their study (Eq. 2a), because oxidation of H_2O_2 requires prior coordination of peroxide to the metal to initiate inner-sphere electron transfer but FeO_4^{2-}, owing to a slower oxygen exchange rate [8] compared to that of its protonated counterparts (i.e., $HFeO_4^-$, H_2FeO_4, and $H_3FeO_4^+$), could not achieve such ligand-substitution, let alone the electron-transfer process afterwards [20].

The newly formed Fe(IV) species can undergo dimerization to form di-Fe(IV) (Eq. 3) and then subsequently self-decomposed to Fe(III) and H_2O_2 (Eq. 4), based on the kinetic study of Fe(IV)-pyrophosphate complex by the pulse radiolysis at pH 10.0 [29]. The reaction rate constants of Equations 3 and 4 at pH 9.0 were estimated to be similar to the reported values at pH 10.0 in the phosphate buffer solution. Fe(IV) oxidation of H_2O_2 (Eq. 5) has only been studied at acidic pH 0 (i.e., $Fe^{IV}O^{2+}$ + H_2O_2, k = 1.0 × 10^4 $M^{-1}{\cdot}s^{-1}$) [30] or at pH 10 in 0.1 M pyrophosphate (Fe(IV)-pyrophosphate complex + H_2O_2, k = 3.9 × 10^5 $M^{-1}{\cdot}s^{-1}$) [29]. Since the speciation of Fe(IV) under different pH conditions is poorly known (pK_a = 9.6 for Fe(IV)-pyrophosphate complex [29]), it is difficult to quantify the pH effect on k_5 in phosphate-buffered condition in our study. Based on the sensitivity analysis of k_5 in the Fe (VI) decay model (Fig. S4), the lower bound (1.0 × 10^4 $M^{-1}{\cdot}s^{-1}$) was found to best fit the experimental data, especially for H_2O_2 generation. This estimated value is also aligned well with the reaction rate constant between Fe(V) and H_2O_2 (k_{10} = 4.0 × 10^5 $M^{-1}{\cdot}s^{-1}$ [31]), which was usually 1–2 orders of magnitude higher than its Fe(IV) counterpart [32]. Fe(IV) can also react with Fe(II) (Eq. 6) in acidic perchlorate and alkaline pyrophosphate solutions and the reported rate constants between Fe(IV) and Fe(II) were 3.56 × 10^4 $M^{-1}{\cdot}s^{-1}$ ($Fe^{IV}O^{2+}$ + Fe(II) at pH 1.0 [33]) and 1.6 × 10^6 $M^{-1}{\cdot}s^{-1}$ (Fe(IV)-pyrophosphate complex + Fe(II) at pH 10.0 [29]), respectively. Based on the sensitivity analysis of k_6 (Fig. S5), Fe(VI) decay and H_2O_2 generation were independent of the magnitude of k_6 ranged from 3.56 × 10^4 $M^{-1}{\cdot}s^{-1}$ to 1.6 × 10^6 $M^{-1}{\cdot}s^{-1}$, thus k_6 was estimated to be ~10^6 $M^{-1}{\cdot}s^{-1}$, closer to the upper limit.

The reaction between Fe(VI) and Fe(II) (Eqs. 7a and 7b) was considered to be the bridge between different iron species, where Fe(V) and Fe(III) were the end products. Previous research has evaluated the oxidation of Fe(II) by Fe(VI) using the stopped-flow spectrophotometer at pH 5.0 and its rate constant was much greater than 5.0 × 10^6 $M^{-1}{\cdot}s^{-1}$ [11]. Meanwhile, it was found that Fe(II) reduced Fe(VI) at a rate of 10^5 $M^{-1}{\cdot}s^{-1}$ at alkaline condition [34]. Based on the sensitivity analysis of k_{7a} (Fig. S6), Fe(VI) decay and H_2O_2 generation

Table 3
Reactions of self-decay of Fe(VI) at pH 9.0.

Reactions	k at pH 9.0	Refs.
[1a] $Fe^{VI}O_4^{2-} + H_2O \rightarrow Fe^{IV}O_3^{2-} + H_2O_2$	$4.8 \times 10^{-5}\ s^{-1}$	This study
[1b] $HFe^{VI}O_4^{-} + HFe^{VI}O_4^{-} + 2\ OH^- \rightarrow Fe_2^{IV}O_6^{4-} + 2\ H_2O_2$	$26\ M^{-1}s^{-1}$	[11]
[2a] $Fe^{VI}O_4^{2-} + H_2O_2 \rightarrow Fe^{IV}O_3^{2-} + O_2 + H_2O$	$\sim 0\ M^{-1}s^{-1}$	[20]
[2b] $HFe^{VI}O_4^{-} + H_2O_2 + OH^- \rightarrow Fe^{IV}O_3^{2-} + O_2 + 2\ H_2O$	$1.7 \times 10^{2}\ M^{-1}s^{-1}$	[20]
[3] $Fe^{IV}O_3^{2-} + Fe^{IV}O_3^{2-} \rightarrow Fe_2^{IV}O_6^{4-}$	$\sim 10^{7}\ M^{-1}s^{-1}$	[29]
[4] $Fe_2^{IV}O_6^{4-} + 4H_2O + 4H^+ \rightarrow 2Fe^{III}(OH)_3(H_2O) + H_2O_2$	$10^{2}\ s^{-1}$	[29]
[5] $Fe^{IV}O_3^{2-} + H_2O_2 + 2H^+ \rightarrow Fe^{II}(OH)_2(aq) + O_2 + 2H_2O$	$1.0 \times 10^{4}\ M^{-1}s^{-1}$	[29,30]
[6] $Fe^{IV}O_3^{2-} + Fe^{II}(OH)_2(aq) + 3\ H_2O \rightarrow 2\ Fe^{III}(OH)_3(aq) + 2\ OH^-$	$\sim 10^{6}\ M^{-1}s^{-1}$	[29]
[7a] $Fe^{VI}O_4^{2-} + Fe^{II}(OH)_2(aq) + H_2O \rightarrow HFe^{V}O_4^{2-} + Fe^{III}(OH)_3(aq)$	$\sim 10^{5}\ M^{-1}s^{-1}$	[11,34]
[7b] $HFe^{VI}O_4^{-} + Fe^{II}(OH)_2(aq) + OH^- \rightarrow HFe^{V}O_4^{2-} + Fe^{III}(OH)_3(aq)$	$\sim 10^{7}\ M^{-1}s^{-1}$	[11]
[8] $Fe^{II}(OH)_2(aq) + H_2O_2 + 2\ OH^- \rightarrow Fe^{IV}O_3^{2-} + 3\ H_2O$	$\sim 10^{2}\ M^{-1}s^{-1}$	[35]
[9a] $HFe^{V}O_4^{2-} + 2H^+ + 4\ H_2O \rightarrow Fe^{III}(OH)_3(H_2O)_3 + H_2O_2$	$5.0\ s^{-1}$	[37]
[9b] $HFe^{V}O_4^{2-} + HFe^{V}O_4^{2-} + 4H_2O + 4H^+ \rightarrow 2\ Fe^{III}(OH)_3(H_2O) + 2\ H_2O_2$	$1.5 \times 10^{7}\ M^{-1}s^{-1}$	[36]
[10] $HFe^{V}O_4^{2-} + H_2O_2 + H_2O \rightarrow Fe^{III}(OH)_3(aq) + O_2 + 2\ OH^-$	$4.0 \times 10^{5}\ M^{-1}s^{-1}$	[20]

Note: Since there was limited information about Fe(IV) speciation, $Fe^{IV}O_3^{2-}$ is the proposed chemical formula of Fe(IV) and reactions 3–6 and 8 from previous work are modified accordingly in this study.

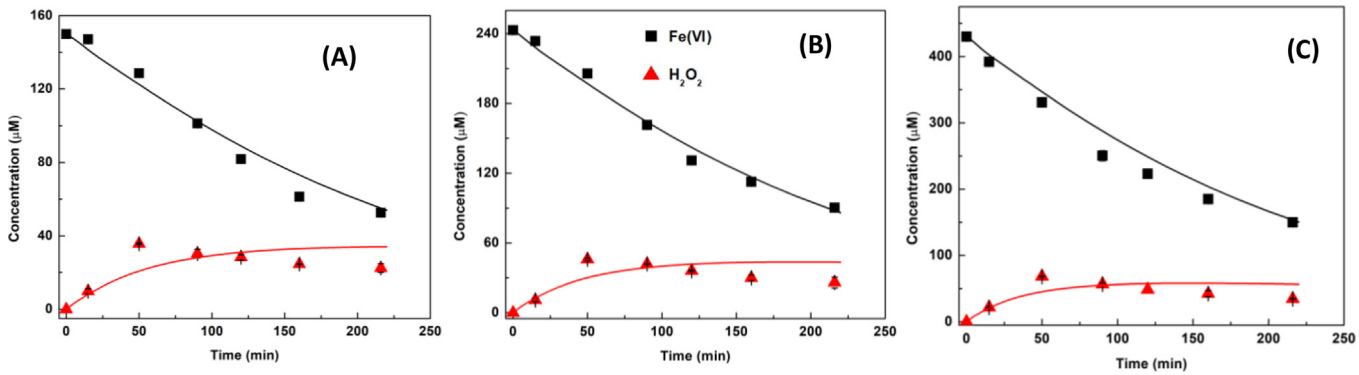

Fig. 2. Measured and predicted H_2O_2 formation and Fe(VI) disappearance during Fe(VI) decay in a phosphate buffer (10.0 mM) at pH 9.0 for varying initial Fe(VI) concentrations. $[Fe(VI)]_0 = 150.0$ (A), 243.0 (B) and 430.0 μM (C); $n = 2$; Symbols: measured data; Lines: model calculation. Error bars represent one standard deviation of data.

were independent of the magnitude of k_{7a} ranged from $10^4\ M^{-1}{\cdot}s^{-1}$ to $10^8\ M^{-1}{\cdot}s^{-1}$. Therefore, an estimated rate constant ($\sim 10^5\ M^{-1}{\cdot}s^{-1}$) was assigned to this reaction (Eq. 7a), which is one order of magnitude lower than its Fe(IV) counterpart k_6 and two orders of magnitudes lower than its mono-protonated Fe(VI) counterpart k_{7b} ($\sim 10^7\ M^{-1}{\cdot}s^{-1}$, Eq. 7b) validated by model simulations in a previous study [11]. Fe(II) was also speculated to generate Fe(IV) in the presence of H_2O_2 (Eq. 8) in the Fenton system at neutral pH condition, and the rate constant between Fe(II) and H_2O_2 was reported to be $5.9 \times 10^3\ M^{-1}{\cdot}s^{-1}$ at pH 7.0 [35] with very limited information under alkaline conditions. Based on the sensitivity analysis of k_8 (Fig. S7), Fe(VI) decay and H_2O_2 generation were independent of the magnitude of k_8 ranged from $0\ M^{-1}\ s^{-1}$ to $10^4\ M^{-1}{\cdot}s^{-1}$ and started to shift when k_8 was increased to $10^5\ M^{-1}{\cdot}s^{-1}$ or higher. Thus, k_8 was estimated to be around $10^2\ M^{-1}{\cdot}s^{-1}$, closer to the lower bound. This also indicated the regeneration of Fe(IV) from Fe(II) could be neglected during Fe(VI) self-decay, considering the relatively small k_8 value observed in Fenton reaction at neutral pH condition [35].

Fe(V) self-decay kinetics also differ in different pH conditions due to its speciation: $H_3Fe^{V}O_4 \rightleftharpoons H^+ + H_2Fe^{V}O_4^-$, $5.5 \le pK_{a1} \le 6.5$; $H_2Fe^{V}O_4^- \rightleftharpoons H^+ + HFe^{V}O_4^{2-}$, $pK_{a2} \approx 7.2$; $HFe^{V}O_4^{2-} \rightleftharpoons H^+ + Fe^{V}O_4^{3-}$, $pKa_3 = 10.1$ [36]. Based on the pulse-radiolysis study of Fe(V) decay in alkaline condition [36], 1st-order kinetics were found to dominate the decay path at pH > 11, while the 2nd-order decay was found to outcompete its 1st-order decay at lower pH (< 11). Later, one study of Fe(V) decay under neutral and acidic conditions found that bimolecular reaction (2nd-order decay) only occurred between $HFeO_4^{2-}$ and FeO_4^{3-} at pH 10–12, while unimolecular reaction (1st-order decay) became the only path for $HFeO_4^{2-}$, $H_2FeO_4^-$, and H_3FeO_4 at pH < 7 [37]. These phenomena were similar to the Fe(VI) decay, where it follows the 1st-order kinetics at very acidic pH [12] (e.g., pH 1.0) and alkaline pH (this study), while the 2nd-order kinetics become the major pathway in neutral conditions [11,18]. Since $HFeO_4^{2-}$ is the major species for Fe(V) at pH 9.0 (i.e., $pK_{a2} = 7.5$ and $pK_{a3} = 10.1$) [36], 1st-order decay (Eq. 9a) and 2nd-order decay (Eq. 9b) were both included to account for the mixed-order decay. However, Equation 9b contributed little to the H_2O_2 generation because Fe(V) concentration was far lower than 3.3×10^{-7} M (ratio of k_{9a} and k_{9b}) under our experimental conditions. More detailed discussion about Equation 9b sensitivity analysis is available in Text S3 and Figs. S8 and S9.

The resultant Fe(V) can also react with H_2O_2 [20] (Eq. 10) and their reactions have been determined previously by the premix pulse-radiolysis technique with a rate constant of $4 \times 10^5\ M^{-1}{\cdot}s^{-1}$ at pH 9.0.

This kinetic model was applied to predict the Fe(VI) disappearance and H_2O_2 generation during Fe(VI) self-decay at pH 9.0 under various experimental conditions. Overall, the model prediction agreed well with the experimental data according to the Theil's inequality coefficient (Text S4 and Table S5). Fig. 2 shows the generation of H_2O_2 and disappearance of Fe(VI) as a function of reaction time up to 216 min at different initial Fe(VI) concentrations. H_2O_2 concentration gradually increased during the first 100 min and maintained at a relatively stable level until 216 min. The prediction by the kinetic model successfully captured the experimental data trends, confirming the robustness of this model.

4. Conclusions

This study addresses the knowledge gap regarding the behavior of

Fe(VI) self-decay under alkaline conditions by elucidating the reaction kinetics and mechanisms. Results strongly indicate that the self-decomposition of FeO_4^{2-} (dominant at alkaline pH 9.0–10.0 condition) in aqueous solution follows 1st-order kinetics and occurs via WA to form the O-O bond, which can liberate H_2O_2 molecule after the generation of Fe(IV). This initial step is followed by other iron intermediate species' (i.e., Fe(V) and Fe(IV)) reactions with H_2O and H_2O_2. The kinetic model based on the reactions amongst Fe(VI), Fe(V), and Fe(IV) can successfully predict the H_2O_2 generation trend, validating the involvement of Fe(V) and Fe(IV) during Fe(VI) decay and the robustness of the kinetic model.

The findings of this study also provide a critical basis for the attempt to simulate intermediate iron species (Fe(V) and Fe(IV)) during Fe(VI) oxidation in more complicated alkaline systems (e.g., wastewater [38] and hydrolyzed human urine [7]). For example, the kinetic model and mechanistic knowledge from this study can be further expanded and adapted for wastewater treatment systems, in which Fe(VI) oxidation of contaminants with or without activators is conducted [4,38,39], and is being pursued with ongoing studies.

Declaration of Competing Interest

The authors declare that they have no known competing financial interests or personal relationships that could have appeared to influence the work reported in this paper.

Acknowledgement

This study was supported by National Science Foundation Grants CBET 1802944 and CBET 1802800. Any opinions, findings, and conclusions or recommendations expressed in this material are those of the authors and do not necessarily reflect the views of the National Science Foundation.

Appendix A. Supplementary data

Supplementary data to this article can be found online at https://doi.org/10.1016/j.cej.2020.124134.

References

[1] R.H. Wood, The heat, free energy and entropy of the ferrate(VI) ion, J. Am. Chem. Soc. 80 (1958) 2038–2041.
[2] M. Feng, C. Jinadatha, T.J. McDonald, V.K. Sharma, Accelerated oxidation of organic contaminants by ferrate(VI): The overlooked role of reducing additives, Environ. Sci. Technol. 53 (2018) 2695–2704.
[3] M. Feng, J.C. Baum, N. Nesnas, Y. Lee, C.-H. Huang, V.K. Sharma, Oxidation of sulfonamide antibiotics of six-membered heterocyclic moiety by ferrate(VI): Kinetics and mechanistic insight into SO_2 extrusion, Environ. Sci. Technol. 53 (2019) 2695–2704.
[4] B. Shao, H. Dong, B. Sun, X. Guan, Role of ferrate(IV) and ferrate(V) in activating ferrate(VI) by calcium sulfite for enhanced oxidation of organic contaminants, Environ. Sci. Technol. 53 (2019) 894–902.
[5] T. Yang, L. Wang, Y. Liu, Z. Huang, H. He, X. Wang, J. Jiang, D. Gao, J. Ma, Comparative study on ferrate oxidation of BPS and BPAF: Kinetics, reaction mechanism, and the improvement on their biodegradability, Water Res. 148 (2019) 115–125.
[6] V.K. Sharma, R. Zboril, R.S. Varma, Ferrates: greener oxidants with multimodal action in water treatment technologies, Accounts Chem. Res. 48 (2015) 182–191.
[7] C. Luo, M. Feng, V.K. Sharma, C.-H. Huang, Oxidation of pharmaceuticals by ferrate (VI) in hydrolyzed urine: Effects of major inorganic constituents, Environ. Sci. Technol. 53 (2019) 5272–5281.
[8] H. Goff, R.K. Murmann, Mechanism of isotopic oxygen exchange and reduction of ferrate(VI) ion (FeO_4^{2-}), J. Am. Chem. Soc. 93 (1971) 6058–6065.
[9] W. Wagner, J. Gump, E. Hart, Factors affecting stability of aqueous potassium ferrate(VI) solutions, Anal. Chem. 24 (1952) 1497–1498.
[10] J.D. Carr, P.B. Kelter, A. Tabatabai, D. Splichal, J. Erickson, C. McLaughlin, Properties of ferrate(VI) in aqueous solution: An alternate oxidant in wastewater treatment, in: R.L. Jolley, et al. (1985) 1285–1298.
[11] Y. Lee, R. Kissner, U. von Gunten, Reaction of ferrate(VI) with ABTS and self-decay of ferrate(VI): Kinetics and mechanisms, Environ. Sci. Technol. 48 (2014) 5154–5162.
[12] R. Sarma, A.M. Angeles-Boza, D.W. Brinkley, J.P. Roth, Studies of the di-iron(VI) intermediate in ferrate-dependent oxygen evolution from water, J. Am. Chem. l Soc. 134 (2012) 15371–15386.
[13] G. Chen, W.W. Lam, P.-K. Lo, W.-L. Man, L.-J. Chen, K.-C. Lau, T.-C. Lau, Mechanism of water oxidation by ferrate(VI) at pH 7–9, Chem.-A Europ. J. 24 (2018) 18735–18742.
[14] V.K. Sharma, Potassium ferrate(VI): an environmentally friendly oxidant, Adv. Environ. Res. 6 (2002) 143–156.
[15] B.E. Norcross, W.C. Lewis, H. Gai, N.A. Noureldin, D.G. Lee, The oxidation of secondary alcohols by potassium tetraoxoferrate(VI), Can. J. Chem. 75 (1997) 129–139.
[16] Y. Lee, M. Cho, J.Y. Kim, J. Yoon, Chemistry of ferrate (Fe(VI)) in aqueous solution and its applications as a green chemical, J. Ind. Eng. Chem. 10 (2004) 161–171.
[17] V.K. Sharma, C.R. Burnett, F.J. Millero, Dissociation constants of the monoprotic ferrate(VI) ion in NaCl media, Phys. Chem. Chem. Phys. 3 (2001) 2059–2062.
[18] Y. Jiang, J.E. Goodwill, J.E. Tobiason, D.A. Reckhow, Effect of different solutes, natural organic matter, and particulate Fe(III) on ferrate(VI) decomposition in aqueous solutions, Environ. Sci. Technol. 49 (2015) 2841–2848.
[19] H. Goff, R. Muermann, Mechanism of isotopic oxygen exchange and reduction of ferrate(VI) ion (FeO_4^{2-}), J. Am. Chem. Soc. 93 (1971) 6058–6065.
[20] J.D. Rush, Z. Zhao, B.H. Bielski, Reaction of ferrate(VI)/ferrate(V) with hydrogen peroxide and superoxide anion-A stopped-flow and premix pulse radiolysis study, Free Radical Res. 24 (1996) 187–198.
[21] M.L. Hoppe, E. Schlemper, R. Murmann, Structure of dipotassium ferrate(VI), Acta Crystallogr. B 38 (1982) 2237–2239.
[22] V.K. Sharma, L. Chen, R. Zboril, Review on high valent Fe^{VI} (ferrate): a sustainable green oxidant in organic chemistry and transformation of pharmaceuticals, ACS Sus. Chem. Eng. 4 (2015) 18–34.
[23] L. Ma, W.W. Lam, P.K. Lo, K.C. Lau, T.C. Lau, Ca^{2+}-induced oxygen generation by FeO_4^{2-} at pH 9–10, Angew. Chem. Int. Ed. 55 (2016) 3012–3016.
[24] X. Yang, M.-H. Baik, *cis*,*cis*-$[(bpy)_2R^{uV}O]_2O^{4+}$ catalyzes water oxidation formally via in situ generation of radicaloid $Ru^{IV}-O^{\bullet}$, J. Am. Chem. Soc. 128 (2006) 7476–7485.
[25] E.M. Sproviero, J.A. Gascón, J.P. McEvoy, G.W. Brudvig, V.S. Batista, Computational studies of the O_2-evolving complex of photosystem II and biomimetic oxomanganese complexes, Coordin. Chem. Rev. 252 (2008) 395–415.
[26] A.E. Clark, J.K. Hurst, Mechanisms of water oxidation catalyzed by ruthenium coordination complexes, Prog. Inorg. Chem. 57 (2011) 1–54.
[27] D.E. Polyansky, J.T. Muckerman, J. Rochford, R. Zong, R.P. Thummel, E. Fujita, Water oxidation by a mononuclear ruthenium catalyst: characterization of the intermediates, J. Am. Chem. Soc. 133 (2011) 14649–14665.
[28] W. Sameera, C.J. McKenzie, J.E. McGrady, On the mechanism of water oxidation by a bimetallic manganese catalyst: a density functional study, Dalton T. 40 (2011) 3859–3870.
[29] J.D. Melton, B.H. Bielski, Studies of the kinetic, spectral and chemical properties of Fe(IV) pyrophosphate by pulse radiolysis, Int. J. Radiat. Appl. Instrum. C Radiat. Phys. Chem. 36 (1990) 725–733.
[30] T. Loegager, J. Holcman, K. Sehested, T. Pedersen, Oxidation of ferrous ions by ozone in acidic solutions, Inorg. Chem. 31 (1992) 3523–3529.
[31] V.K. Sharma, Oxidation of inorganic compounds by ferrate(VI) and ferrate(V): One-electron and two-electron transfer steps, Environ. Sci. Technol. 44 (2010) 5148–5152.
[32] V.K. Sharma, Oxidation of inorganic contaminants by ferrates(VI, V, and IV)–kinetics and mechanisms: a review, J. Environ. Manage. 92 (2011) 1051–1073.
[33] O. Pestovsky, A. Bakac, Aqueous ferryl(IV) ion: Kinetics of oxygen atom transfer to substrates and oxo exchange with solvent water, Inorg. Chem. 45 (2006) 814–820.
[34] V.K. Sharma, B.H. Bielski, Reactivity of ferrate(VI) and ferrate(V) with amino acids, Inorg. Chem. 30 (1991) 4306–4310.
[35] H. Bataineh, O. Pestovsky, A. Bakac, pH-induced mechanistic changeover from hydroxyl radicals to iron(IV) in the Fenton reaction, Chem. Sci. 3 (2012) 1594–1599.
[36] J. Rush, B.H. Bielski, Kinetics of ferrate(V) decay in aqueous solution. A pulse-radiolysis study, Inorg. Chem. 28 (1989) 3947–3951.
[37] J.D. Rush, B.H. Bielski, Decay of ferrate(V) in neutral and acidic solutions. A premix pulse radiolysis study, Inorg. Chem. 33 (1994) 5499–5502.
[38] K. Manoli, L.M. Morrison, M.W. Sumarah, G. Nakhla, A.K. Ray, V.K. Sharma, Pharmaceuticals and pesticides in secondary effluent wastewater: Identification and enhanced removal by acid-activated ferrate(VI), Water Res. 148 (2019) 272–280.
[39] M. Feng, V.K. Sharma, Enhanced oxidation of antibiotics by ferrate(VI)-sulfur(IV) system: Elucidating multi-oxidant mechanism, Chem. Eng. J. 341 (2018) 137–145.